Green's function approach to the Kondo effect in nanosized quantum corrals

Q. L. Li,[1] R. Wang,[1,2] K. X. Xie,[1] X. X. Li,[1] C. Zheng,[1] R. X. Cao,[1,3] B. F. Miao,[1,4] L. Sun,[1,4] B. G. Wang,[1,4,*] and H. F. Ding[1,4,†]

[1]*National Laboratory of Solid State Microstructures and Department of Physics, Nanjing University, 22 Hankou Road, Nanjing 210093, People's Republic of China*

[2]*Department of Physics and Astronomy, Shanghai Jiao Tong University, Shanghai 200240, People's Republic of China*

[3]*College of Physics Science and Technology, Yangzhou University, Yangzhou 225002, People's Republic of China*

[4]*Collaborative Innovation Center of Advanced Microstructures, Nanjing University, 22 Hankou Road, Nanjing 210093, People's Republic of China*

(Received 5 February 2018; revised manuscript received 22 March 2018; published 2 April 2018)

We present a theoretical study of the Kondo effect for a magnetic atom placed inside nanocorrals using Green's function calculations. Based on the standard mapping of the Anderson impurity model to a one-dimensional chain model, we formulate a weak-coupling theory to study the Anderson impurities in a hosting bath with a surface state. With further taking into account the multiple scattering effect of the surrounding atoms, our calculations show that the Kondo resonance width of the atom placed at the center of the nanocorral can be significantly tuned by the corral size, in good agreement with recent experiments [Q. L. Li *et al.*, Phys. Rev. B **97**, 035417 (2018)]. The method can also be applied to the atom placed at an arbitrary position inside the corral where our calculation shows that the Kondo resonance width also oscillates as the function of its separation from the corral center. The prediction is further confirmed by the low-temperature scanning tunneling microscopy studies where a one-to-one correspondence is found. The good agreement with the experiments validates the generality of the method to the system where multiadatoms are involved.

DOI: 10.1103/PhysRevB.97.155401

I. INTRODUCTION

The Kondo effect is one of the most studied electron correlation phenomena in condensed matter physics [1]. It describes the spin of magnetic impurity in a nonmagnetic host interacting with the spins of surrounding conduction electrons. The effect was discovered in the 1930s [2] and then later explained by Kondo [3]. At low temperature, a many-body nonmagnetic singlet ground state is formed, resulting in a spectroscopic signature around the Fermi level of the host, i.e., the Kondo [3] or Abrikosov-Suhl [4,5] resonance. To date, the resonance has been investigated down to a single atom or single molecular level with low-temperature scanning tunneling spectroscopy (STS) [6–15].

Quantum corrals exhibit rich physical phenomena, such as the enhancement of the switching probability of tautomerization [16]; the regulation of adatom diffusion, self-assembly, and atom trapping [17–21]; the modulation of Ruderman-Kittel-Kasuya-Yosida (RKKY) interaction [22,23]; the single-atom gating of quantum-state superpositions [24]; and the electronic structure inversion of an adatom [25], etc. When the Kondo effect encounters elliptical quantum corrals, the Kondo effect created by the adatom at one focus can even be projected to the other focus where no adatom is present; that is, the quantum mirage emerges [7]. Many different theoretical approaches have successfully reproduced the quantum mirage phenomenon [26–29]. The discussion of the variation of the Kondo temperature as a function of the corral diameters or the positions in corrals, however, is still rare. A theoretical work investigated the Kondo effect of a magnetic adatom placed in a circular quantum corral built in a two-dimensional system where the bulk state is absent and predicted that the Kondo effect is spatially dependent [30]. In fact, whether and how the surface state influences the Kondo temperature have been in hot debate for a certain time [8,31–36]. Recent experimental observation showed that the Kondo temperature of Co adatoms placed at the center of nanocorrals on the surface of Ag(111) oscillates strongly as a function of the diameter of the corral built by multiadatoms [37]. The understanding of the effect demands a theory to describe the Kondo effect in the condition that multiadatoms are involved.

In order to address the complicated situation where multiple magnetic impurities are adsorbed on the surface of noble metals, we construct a theory based on the duality between strong- and weak-coupling limit in the Anderson impurity model [1,38–40]. The multiple impurities on the surface are discussed by considering the renormalization effect due to the interadatom couplings. Our calculations not only reproduce the recent experimental finding of the oscillations of the Kondo resonance width (the half width of the half maximum of the Kondo resonance peak) versus the quantum corral size but also predict that it should also oscillate as a function of the separation from the quantum corral center. We further performed low-temperature STS measurements and found one-to-one correspondence with the prediction. The good agreement between the theory and experiments demonstrates

*bgwang@nju.edu.cn
†hfding@nju.edu.cn

the validity of our approach to the Kondo problems with the involvement of multiadatoms.

The paper is organized as follows. In Sec. II, we describe the microscopic theory with three subsections. In Sec. II A, we first take a single magnetic impurity as a starting point and briefly review the strong- and weak-coupling duality in the Anderson impurity model [1,39,40]. After that, we generalize it to the case where both surface and bulk degrees of freedom exist. Within this formalism, we are able to extract the Kondo resonance width in a more realistic situation where both the surface and the bulk states are present. In Sec. II B, we discuss the multiple-impurity case. It is known that even though more precise methods, such as the numerical renormalization group (NRG), have been developed to understand single (or a few) impurity cases, the general way to deal with any multiple-impurity models requiring much less computational effort is still needed. Due to the merit of the duality of the weak-coupling model, we can readily generalize the above framework to include multiple impurities. This allows general applications to any models with generic distribution of impurities. As will be shown in Sec. V, this method explains our experimental findings satisfactorily (see Sec. V). Section II C briefly summarizes the calculation of the local density of states (LDOS) in the presence of multiple impurities, which we adopted from Refs. [41–43]. In Sec. III, we apply our method to calculate the case for a Co adatom placed at the vicinity of another Co adatom and compare it with the experimental result. Section IV is dedicated to the calculation of the Kondo resonance width of a Co adatom placed at arbitrary positions of nanocorrals with different diameters. Section V shows the one-to-one comparison of the calculated and experimental values of Kondo resonance width for the Co adatom placed at the center of the nanocorral as a function of the corral diameter and placed at an arbitrary position inside corrals of given sizes. Finally, a brief summary of our main findings is given in Sec. VI.

II. MICROSCOPIC THEORY

A. Duality between strong and weak coupling in surface-mediated Kondo effect

We start with the simplest case where a single quantum impurity is immersed in the bulk-conduction electron bath. The relevant physics including both the magnetic moment and the charge fluctuation can all be contained in the standard Anderson model [38],

$$H = \sum_{\mathbf{q}\sigma} (\varepsilon_{\mathbf{q}\sigma} - \varepsilon_F) c^\dagger_{\mathbf{q}\sigma} c_{\mathbf{q}\sigma} + \sum_{\mathbf{q}\sigma} (V_b c^\dagger_{\mathbf{q}\sigma} d_\sigma + V_b^* d^\dagger_\sigma c_{\mathbf{q}\sigma}) + \sum_\sigma \varepsilon_d d^\dagger_\sigma d_\sigma + U \sum_\sigma n_\sigma n_{\bar\sigma}. \quad (1)$$

where the first term describes the free bulk-conduction electron bath, the second term is the hybridization between bulk state and localized impurity state, the third term is the impurity-state electron, and the fourth term is the contribution of double-occupied energy. We focus our discussion on the Kondo limit, where the impurity can manifest itself by a finite local magnetic moment. This means that we focus on the parameter region, $\varepsilon_d < \varepsilon_F < \varepsilon_d + U$, where the empty and the double-occupancy states of the local impurity are forbidden, and also $U \gg \Gamma$, with $\Gamma = \pi \sum_{\mathbf{q}} |V_b|^2 \delta(\varepsilon_F - \varepsilon_{\mathbf{q}\sigma})$, where the charge fluctuation is suppressed. In this Kondo limit, it is well known that Eq. (1) is equivalent to the Kondo exchange model [3] with interaction J, through the Schrieffer-Wolff transformation [44]. Following a renormalization group analysis [40], two fixed points can be found for the antiferromagnetic Kondo model, i.e., $J = 0$ and $J = \infty$. As we are interested in the Kondo effect, we only consider the stable strong-coupling fixed point $J = \infty$. At $J = \infty$, within the NRG formalism, the Kondo Hamiltonian is mapped to a one-dimensional (1D) chain with infinite exchange coupling at one boundary. Since the impurity site is strongly coupled to the first conduction electron site in the 1D chain, the physical excitations including the impurity site are all effectively frozen at the strong-coupling fixed point. Therefore, the most relevant operators will be the Hubbard-type interaction at the first site and the hybridization term between the first several sites. Due to this reason, the large U ($U \gg \Gamma$) Anderson model in Eq. (1) can be mapped into a weak-coupling effective Anderson model, which reads as

$$H_{\text{eff}} = \sum_{\mathbf{q}\sigma} (\varepsilon_{\mathbf{q}\sigma} - \varepsilon_F) c^\dagger_{\mathbf{q}\sigma} c_{\mathbf{q}\sigma} + \sum_{\mathbf{q}\sigma} (\tilde V_b c^\dagger_{\mathbf{q}\sigma} d_\sigma + \tilde V_b^* d^\dagger_\sigma c_{\mathbf{q}\sigma}) + \sum_\sigma \tilde\varepsilon_d d^\dagger_\sigma d_\sigma + \tilde U \sum_\sigma n_\sigma n_{\bar\sigma}. \quad (2)$$

d_σ is the operator representing the first site of the conduction electron in the NRG chain. It describes the high-energy effective fermionic degrees of freedom that couple most strongly to the impurity. As discussed before, the parameters $\tilde V_b$, $\tilde\varepsilon_d$, and $\tilde U$ are all renormalized in the strong-coupling limit. $\tilde\varepsilon_d$ is the Fermi energy of the conduction electron at the first site of the 1D chain, i.e., $\tilde\varepsilon_d = \varepsilon_F$. $\tilde U$ is renormalized to a weak interaction compared to $\varepsilon_{\mathbf{q}\sigma}$ and can be treated perturbatively.

Let us now shift our attention to the surface degrees of freedom in noble metals. In a more realistic situation where a single impurity is deposited onto a noble metal surface, both the surface and bulk states could have nonzero hybridization with the adatom. To this end, Eq. (1) should be generalized to the following form,

$$H = \sum_{\mathbf{k}\sigma} (\varepsilon_{\mathbf{k}\sigma} - \varepsilon_F) c^\dagger_{\mathbf{k}\sigma} c_{\mathbf{k}\sigma} + \sum_{\mathbf{k}\sigma} (V_s c^\dagger_{\mathbf{k}\sigma} d_\sigma + V_s^* d^\dagger_\sigma c_{\mathbf{k}\sigma}) + \sum_{\mathbf{q}\sigma} (\varepsilon_{\mathbf{q}\sigma} - \varepsilon_F) c^\dagger_{\mathbf{q}\sigma} c_{\mathbf{q}\sigma} + \sum_{\mathbf{q}\sigma} (V_b c^\dagger_{\mathbf{q}\sigma} d_\sigma + V_b^* d^\dagger_\sigma c_{\mathbf{q}\sigma}) + \sum_\sigma \varepsilon_d d^\dagger_\sigma d_\sigma + U \sum_\sigma n_\sigma n_{\bar\sigma}, \quad (3)$$

where $\mathbf{k}$ and $\mathbf{q}$ represent the wave vectors of the surface and bulk bands, respectively. $c_{\mathbf{k}\sigma}$ ($c_{\mathbf{q}\sigma}$) is the annihilation operator of the surface (bulk) electrons. V_s (V_b) is the hybridization constant between the surface (bulk) state and the impurity, and we assume the orthogonality between the surface and bulk states, namely, $\langle 0 | c_{\mathbf{k}\sigma} c^\dagger_{\mathbf{q}\sigma'} | 0 \rangle = 0$. Following the same procedure above, the duality between the strong- and weak-coupling limit allows us to map Eq. (3) to the effective model

in the low-energy window as

$$H_{\text{eff}} = \sum_{\mathbf{k}\sigma} (\varepsilon_{\mathbf{k}\sigma} - \varepsilon_F) c^\dagger_{\mathbf{k}\sigma} c_{\mathbf{k}\sigma} + \sum_{\mathbf{k}\sigma} (\tilde{V}_s c^\dagger_{\mathbf{k}\sigma} d_\sigma + \tilde{V}^*_s d^\dagger_\sigma c_{\mathbf{k}\sigma}) + \sum_{\mathbf{q}\sigma} (\varepsilon_{\mathbf{q}\sigma} - \varepsilon_F) c^\dagger_{\mathbf{q}\sigma} c_{\mathbf{q}\sigma} + \sum_{\mathbf{q}\sigma} (\tilde{V}_b c^\dagger_{\mathbf{q}\sigma} d_\sigma + \tilde{V}^*_b d^\dagger_\sigma c_{\mathbf{q}\sigma}) + \sum_\sigma \tilde{\varepsilon}_d d^\dagger_\sigma d_\sigma + \tilde{U} \sum_\sigma n_\sigma n_{\bar{\sigma}}. \quad (4)$$

Similar to the standard case, $\tilde{\varepsilon}_d = \varepsilon_F$, and $\tilde{U}$ is no longer the strong coupling in the above Eq. (3), but is a weak interaction that can be treated by the perturbation theory.

To study Eq. (4), one can calculate the equation of motion of the Green's function (GF). Using the Hartree-Fock approximation, the retarded GF of the d_σ field reads as

$$G^{-1}_{d_\sigma d_\sigma} = \omega - \tilde{\varepsilon}_d - U\langle n_{d\bar{\sigma}}\rangle - \sum_{\mathbf{k}} \frac{|\tilde{V}_s|^2}{\omega - \varepsilon_{\mathbf{k}\sigma} + \varepsilon_F + i0^+} - \sum_{\mathbf{q}} \frac{|\tilde{V}_b|^2}{\omega - \varepsilon_{\mathbf{q}\sigma} + \varepsilon_F + i0^+}. \quad (5)$$

The real part of the fourth and fifth terms in the above equation is usually negligibly small or can be absorbed into $\tilde{\varepsilon}_d$. The imaginary part gives us the hybridization function due to the surface and bulk states, respectively, with $\tilde{\Delta}_s = \pi|\tilde{V}_s|^2 \sum_{\mathbf{k}} \delta(\omega - \varepsilon_{\mathbf{k}\sigma})$ and $\tilde{\Delta}_b = \pi|\tilde{V}_b|^2 \sum_{\mathbf{q}} \delta(\omega - \varepsilon_{\mathbf{q}\sigma})$. Then, the retarded GF becomes

$$G^{-1}_{d_\sigma d_\sigma} = \omega - \tilde{\varepsilon}_d - \Sigma_\sigma(\omega) + i\tilde{\Gamma}, \quad (6)$$

where $\tilde{\Gamma} = \tilde{\Delta}_s + \tilde{\Delta}_b$, and $\Sigma_\sigma(\omega)$ satisfies $\Sigma_\sigma(\omega) = \tilde{U}\langle n_{\bar{\sigma}}\rangle + \sum_{\mathbf{k}} P(\frac{1}{\omega - \varepsilon_{\mathbf{k}\sigma} + \varepsilon_F}) + \sum_{\mathbf{q}} P(\frac{1}{\omega - \varepsilon_{\mathbf{q}\sigma} + \varepsilon_F}) \approx \tilde{U}\langle n_{\bar{\sigma}}\rangle$. This is the total self-energy received from the hybridization and the Hubbard interaction. Further expanding the self-energy with respect to the Fermi energy, one can readily arrive at

$$G_{d_\sigma d_\sigma}(\omega) = \frac{1}{\omega - \varepsilon_F - \varepsilon'_d + i\tilde{\Gamma}}, \quad (7)$$

where $\varepsilon'_d = z[\tilde{\varepsilon}_d - \varepsilon_F + \Sigma_d(\varepsilon_F)]$, and z is the wave-function weight factor. The above renormalized GF means that in the strong-coupling limit, the Anderson model still enjoys well-defined quasiparticles with a finite lifetime defined by $\tilde{\Gamma}$. This is a result of the weak-coupling effective model after duality mapping, which is well within the description of the Landau Fermi liquid. The density of states at the impurity site then can be obtained as

$$\rho(\omega) = \frac{1}{\pi} \frac{\tilde{\Gamma}}{(\omega - \varepsilon_F - \varepsilon'_d)^2 + \tilde{\Gamma}^2}. \quad (8)$$

Two conclusions are obvious from the above equation. First, since we have $\tilde{\varepsilon}_d = \varepsilon_F$, $\varepsilon'_d = z\Sigma_d(\varepsilon_F)$. Moreover, as discussed above, in the effective model $\tilde{U} \ll U$ and $\tilde{U} \ll \varepsilon_d$; therefore ε'_d is much less than the d-resonance energies, ε_d and $\varepsilon_d + U$ in the original model, Eq. (3). Hence, the center of the Lorentzian peak in Eq. (8), $\omega_0 = \varepsilon_F + \varepsilon'_d$, is far away from the d-resonance energies and is very near to the Fermi energy. This peak is identified to be the Kondo resonance peak, and Eq. (8) means that in the low-energy window, though both surface and bulk states are active, the Kondo resonance would still occur and can be observed near the Fermi energy. Secondly, the Kondo resonance width is determined by $\tilde{\Gamma} = \tilde{\Delta}_s + \tilde{\Delta}_b$, i.e., by contributions from both the surface and the bulk-state electrons. Their contributions can be directly summed up due to the orthogonality between the surface and bulk wave functions.

It is still worthwhile mentioning that the above analysis is based on the strong-weak duality from Eq. (3) to Eq. (4), which is applicable only in the low-temperature regime where both the bulk and surface sectors reach their strong-coupling fixed point. As will be clear below, this is indeed the case in our experiments. In this case, both the surface and the bulk degrees of freedom contribute to the Kondo resonance and the resonance width is proved to be a direct sum of the two terms. For a higher-temperature regime, more care should be taken before using Eq. (4), and two different Kondo temperatures, for the bulk and surface, respectively, may be expected. This is beyond the scope of this work and could be an interesting topic for future study.

B. Surface-mediated Kondo effect in the case of multiple impurities

Having established the framework based on the strong-weak duality, we are ready to consider a complicated case where multiple quantum impurities are randomly distributed on the surface of a noble metal, e.g., Ag(111). Firstly, we consider a system with $(N+1)$ impurities, namely, one test impurity accompanied by N impurities. First, the distance R between any two Co atoms is important, and has been discussed in Refs. [45,46]. It was found that when R is larger than ~0.8 nm, the direct exchange interaction between the local moments of the two Co atoms can be neglected. When the two adatoms are close enough, exchange interaction occurs and suppresses the Kondo effect. In our theory and experiments, the exchange coupling can be neglected since the atoms are well separated. Secondly, since the impurities will hybridize with both the bulk and the surface bands, $2(N+1)$ hybridization terms need to be taken into account in the corresponding Anderson model. Following the same procedure as in the above section, an effective weak-coupling Hamiltonian including $N+1$ impurities can be written as $H = H_0 + H_I$, with

$$H_0 = \sum_{i=0}^{N} \sum_\sigma \left(\varepsilon_d d^\dagger_{i\sigma} d_{i\sigma} + U n^i_\sigma n^i_{\bar{\sigma}}\right) + \sum_{\mathbf{k}\sigma} \xi_{\mathbf{k}\sigma} c^\dagger_{\mathbf{k}\sigma} c_{\mathbf{k}\sigma} + \sum_{\mathbf{q}\sigma} \xi_{\mathbf{q}\sigma} c^\dagger_{\mathbf{q}\sigma} c_{\mathbf{q}\sigma}, \quad (9)$$

and

$$H_I = \sum_{i=0}^{N} \sum_{\mathbf{k}\sigma} (V_s d^\dagger_{i\sigma} c_{\mathbf{k}\sigma} e^{i\mathbf{k}\cdot\mathbf{R}_i} + \text{H.c.}) + \sum_{i=0}^{N} \sum_{\mathbf{q}\sigma} (V_b d^\dagger_{i\sigma} c_{\mathbf{q}\sigma} e^{i\mathbf{q}\cdot\mathbf{R}_i} + \text{H.c.}), \quad (10)$$

where $\mathbf{R}_i$ denotes the real space position of the ith adatom. $\xi_{\mathbf{k}\sigma} = \varepsilon_{\mathbf{k}\sigma} - \varepsilon_F$ and $\xi_{\mathbf{q}\sigma} = \varepsilon_{\mathbf{q}\sigma} - \varepsilon_F$ are the energy spectrum for the bulk and surface excitations, respectively. U is the effective weak interaction between local electrons, where we have neglected the tilde symbol for the purpose of brevity (also for ε_d and the hybridizations V_s, V_b below).

Since we are interested in the propagation of the Kondo resonance via the surface state, we consider the situation that there is a particular impurity $i = 0$ which is relatively far away from the N other impurities [Fig. 1]. Let us first study the self-energy correction of a generic atom i ($i \neq 0$). By using the Dyson equation, the dressed Green's function of an adatom i can be obtained from all the other adatoms,

$$G_i'^{-1} = G_i^{-1} - \sum_{j\neq i,0}^{N} \Sigma_{ij}(\omega, R_{ij}), \quad \text{with}$$

$$\Sigma_{ij} \approx \left(V_s^2 \sum_{\mathbf{k}} \frac{e^{-i\mathbf{k}\cdot\mathbf{R}_{ij}}}{\omega^+ - \xi_{\mathbf{k}}}\right) G_i(\omega) \left(V_s^2 \sum_{\mathbf{k}'} \frac{e^{-i\mathbf{k}'\cdot\mathbf{R}_{ij}}}{\omega^+ - \xi_{\mathbf{k}'}}\right). \quad (11)$$

$G_i(\omega) = G_{d_\sigma,d_\sigma}(\omega)$ is the retarded GF of the isolated single adatom. Further, we can simplify Σ_{ij} as the function form $\Sigma_{ij}(\omega, R_{ij}) = \mathrm{Re}\Sigma_{ij}(\omega, R_{ij}) - i\,\mathrm{Im}\Sigma_{ij}(\omega, R_{ij})$ with

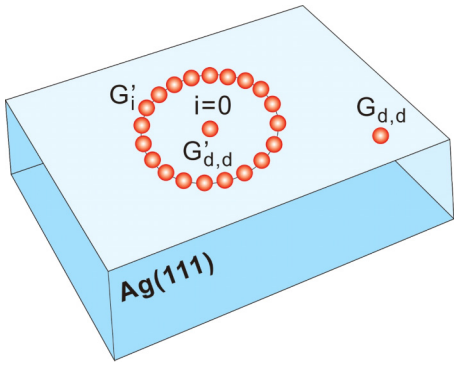

FIG. 1. Sketch of multiple Co adatoms on Ag(111). For an isolated adatom, the Green's function is $G_{d,d}$ (lower right corner) in the text. For an adatom within a corral ($i = 0$) and the adatoms forming the corral ($i \neq 0$), the Green's functions are $G'_{d,d}$ and G'_i in the text, respectively.

$$\mathrm{Re}\Sigma_{ij}(\omega, R_{ij}) = \frac{[\omega - \varepsilon_d - \mathrm{Re}\Sigma(\omega)]\left[I_1^2(\omega, R_{ij}) - I_2^2(\omega, R_{ij})\right] - 2I_1(\omega, R_{ij})I_2(\omega, R_{ij})\mathrm{Im}\Sigma(\omega)}{[\omega - \varepsilon_d - \mathrm{Re}\Sigma(\omega)]^2 + \mathrm{Im}\Sigma(\omega)^2}, \quad (12)$$

and

$$\mathrm{Im}\Sigma_{ij}(\omega, R_{ij}) = \frac{\mathrm{Im}\Sigma(\omega)\left[I_1^2(\omega, R_{ij}) - I_2^2(\omega, R_{ij})\right] + 2I_1(\omega, R_{ij})I_2(\omega, R_{ij})[\omega - \varepsilon_d - \mathrm{Re}\Sigma(\omega)]}{[\omega - \varepsilon_d - \mathrm{Re}\Sigma(\omega)]^2 + \mathrm{Im}\Sigma(\omega)^2}, \quad (13)$$

with $V_s^2 \sum_{\mathbf{k}} \frac{e^{-i\mathbf{k}\cdot\mathbf{R}}}{\omega^+ - \xi_{\mathbf{k}}} = I_1(R,\omega) - i\,I_2(R,\omega)$ and $R_{ij} = |\mathbf{R}_i - \mathbf{R}_j|$, which is the distance between any two adatoms. Similar separation can be done for the bulk-state sector, $\sum_{\mathbf{q}} \frac{V_b^2}{i\omega_n - \xi_{\mathbf{q}}} e^{-i\mathbf{q}\cdot\mathbf{R}}$. We have checked numerically that the above integral and the final contribution to the self-energy correction from the bulk states is much smaller than that from the surface contributions, and therefore can be neglected. Then, decomposing the self-energy correction into its real and imaginary part, one can arrive at

$$G_i'^{-1} = \omega - \varepsilon_d - \mathrm{Re}\Sigma_i(\omega) + i\,\mathrm{Im}\Sigma_i(\omega), \quad (14)$$

where

$$\mathrm{Re}\Sigma_i(\omega) = \mathrm{Re}\Sigma(\omega) + \mathrm{Re}\sum_{j\neq i}^{N} \Sigma_{ij}(\omega, R_{ij}) \quad (15)$$

and

$$\mathrm{Im}\Sigma_i(\omega) = \mathrm{Im}\Sigma(\omega) + \mathrm{Im}\sum_{j\neq i}^{N} \Sigma_{ij}(\omega, R_{ij}). \quad (16)$$

Now we are ready to consider the intermediate coupling between $i = 0$ and the $i \neq 0$ atoms. Each of the $i \neq 0$ impurities hybridizes with the $i = 0$ impurity via the surface state. One can decompose the problem into a series of two-body models. Then the ith adatom contributes a self-energy correction to the $i = 0$ impurity as

$$\Sigma_i'(\omega, R_{i0}) = \mathrm{Re}\Sigma_i'(\omega, R_{i0}) - i\,\mathrm{Im}\Sigma_i'(\omega, R_{i0}), \quad (17)$$

where

$$\mathrm{Re}\Sigma_i'(\omega, R_{i0}) = \frac{[\omega - \varepsilon_d - \mathrm{Re}\Sigma_i(\omega)]\left[I_1^2(\omega, R_{i0}) - I_2^2(\omega, R_{i0})\right] - 2I_1(\omega, R_{i0})I_2(\omega, R_{i0})\mathrm{Im}\Sigma_i(\omega)}{[\omega - \varepsilon_d - \mathrm{Re}\Sigma_i(\omega)]^2 + \mathrm{Im}\Sigma_i(\omega)^2}, \quad (18)$$

and

$$\mathrm{Im}\Sigma_i'(\omega, R_{i0}) = \frac{\mathrm{Im}\Sigma_i(\omega)\left[I_1^2(\omega, R_{i0}) - I_2^2(\omega, R_{i0})\right] + 2I_1(\omega, R_{i0})I_2(\omega, R_{i0})[\omega - \varepsilon_d - \mathrm{Re}\Sigma_i(\omega)]}{[\omega - \varepsilon_d - \mathrm{Re}\Sigma_i(\omega)]^2 + \mathrm{Im}\Sigma_i(\omega)^2}. \quad (19)$$

After considering all the $i \neq 0$ adatoms, we obtain the total self-energy correction and the final dressed Green's function of the $i = 0$ impurity:

$$G'^{-1}_{d\sigma,d\sigma}(\omega) = G^{-1}_{d\sigma,d\sigma} - \sum_{i=1}^{N} \Sigma'_i(\omega, R_{i0}). \tag{20}$$

Further, Eq. (20) can be written as $G'^{-1}_{d\sigma,d\sigma} = \omega - \varepsilon_d - \mathrm{Re}\Sigma''(\omega) + i\,\mathrm{Im}\Sigma''(\omega)$, with

$$\mathrm{Re}\Sigma'' = \mathrm{Re}\Sigma(\omega) + \sum_{i=1}^{N} \mathrm{Re}\Sigma'_i(\omega, R_{i0}) \tag{21}$$

and

$$\mathrm{Im}\Sigma'' = \mathrm{Im}\Sigma(\omega) + \sum_{i=1}^{N} \mathrm{Im}\Sigma'_i(\omega, R_{i0}). \tag{22}$$

By substituting Eq. (19) into Eq. (22), we arrive at the dressed imaginary part of the self-energy of the $i = 0$ adatom, which reads as

$$\mathrm{Im}\Sigma'' = \mathrm{Im}\Sigma(\omega) + \sum_{i=1}^{N} \frac{\mathrm{Im}\Sigma_i(\omega)\left[I_1^2(\omega, R_{i0}) - I_2^2(\omega, R_{i0})\right] + 2I_1(\omega, R_{i0})I_2(\omega, R_{i0})[\omega - \varepsilon_d - \mathrm{Re}\Sigma_i(\omega)]}{[\omega - \varepsilon_d - \mathrm{Re}\Sigma_i(\omega)]^2 + \mathrm{Im}\Sigma_i(\omega)^2}. \tag{23}$$

Here $\mathrm{Im}\Sigma(\omega) = w_0$ is the single-adatom Kondo resonance width on a wide terrace without perturbation. $\mathrm{Im}\Sigma_i(\omega)$ can be derived from Eq. (16). However, in order to calculate $\mathrm{Im}\Sigma_i(\omega)$, we have to obtain $\Sigma_{ij}(\omega, R_{ij})$ first. It is worthwhile noting that the Kondo resonance of a single Co atom is very close to the Fermi energy, i.e., $\varepsilon_d + \mathrm{Re}\Sigma(\omega) \approx \varepsilon_F$; hence $\Sigma_{ij} \equiv \Sigma_{ij}(\omega, R_{ij})$ is simplified, with

$$\mathrm{Re}\Sigma_{ij} \approx \frac{(\omega - \varepsilon_F)\left[I_1^2(\omega, R_{ij}) - I_2^2(\omega, R_{ij})\right] - 2I_1(\omega, R_{ij})I_2(\omega, R_{ij})w_0}{(\omega - \varepsilon_F)^2 + w_0^2}, \tag{24}$$

and

$$\mathrm{Im}\Sigma_{ij} \approx \frac{w_0\left[I_1^2(\omega, R_{ij}) - I_2^2(\omega, R_{ij})\right] + 2I_1(\omega, R_{ij})I_2(\omega, R_{ij})(\omega - \varepsilon_F)}{(\omega - \varepsilon_F)^2 + w_0^2}. \tag{25}$$

For ω near ε_F, we have $\mathrm{Re}\Sigma_{ij} \approx -2I_1(\omega, R_{ij})I_2(\omega, R_{ij})/w_0$, so $\mathrm{Re}\Sigma_i(\omega) = \varepsilon_F - \varepsilon_d - 2\sum_{j=1}^{N} I_1(\omega, R_{ij})I_2(\omega, R_{ij})$. Further, using $\mathrm{Im}\Sigma_{ij} \approx [I_1^2(\omega, R_{ij}) - I_2^2(\omega, R_{ij})]/w_0$, we finally arrive at

$$\mathrm{Im}\Sigma'' = w_0 + \sum_{i=1}^{N} \frac{\left[I_1^2(\omega, R_{i0}) - I_2^2(\omega, R_{i0})\right]}{w_0 + \frac{1}{w_0}\sum_{j\neq i,0}\left[I_1^2(\omega, R_{ij}) - I_2^2(\omega, R_{ij})\right]}. \tag{26}$$

The above equation includes all the information of the Kondo resonance, as a function of N and the distance between each pair of atoms.

In order to make an actual comparison with experiments, the effect of an STM tip also needs to be taken into consideration, besides the impurities. The STM tip site brings in new terms including the on-site energy of the tip atom, the hybridization between the tip atom and the impurity atom, the surface electrons, and the bulk electrons. All the possible terms can be written as [47,48]

$$H_{\mathrm{tip}} = \sum_{\sigma} V_{td}(d_\sigma^\dagger t_\sigma + \mathrm{H.c.}) + \sum_{\mathbf{k}\sigma} V_{ts}(c_{\mathbf{k}\sigma}^\dagger c_{t\sigma} + \mathrm{H.c.}) + \sum_{\mathbf{q}\sigma} V_{tb}(c_{\mathbf{q}\sigma}^\dagger c_{t\sigma} + \mathrm{H.c.}) + \varepsilon_t t_\sigma^\dagger t_\sigma, \tag{27}$$

where $t_\sigma^\dagger$, t_σ are the creation and annihilation operators of the tip electrons with spin σ. It is then straightforward to calculate the STM tunneling current $I(\mathrm{eV}) = -e\sum_\sigma \langle \frac{d}{dt} t_\sigma^\dagger t_\sigma \rangle$, with the resulting conductance being similar to the Fano resonance [49]. The calculated derivative conductance dI/dV is found to satisfy

$$\frac{dI}{dV} \propto \frac{(\varepsilon + q)^2}{1 + \varepsilon^2}, \tag{28}$$

where q is a parameter that is associated with the ratio between the hybridization with the Co atom and the hybridization with the bulk and surface electrons. The expression ε is derived to be

$$\varepsilon = \frac{\omega - \varepsilon_d - \mathrm{Re}\Sigma''(\omega)}{\mathrm{Im}\Sigma''(\omega)}. \tag{29}$$

From Eqs. (28) and (29), it is known that the width of the predicted Fano resonance should be determined by $\mathrm{Im}\Sigma''$, which is further given by Eq. (26), i.e., $w = \mathrm{Im}\Sigma''(\omega)$. The above calculation starts from a microscopic model that deals with nearly all possible interactions that may dominate in the multiple-atom experiment. Therefore, Eq. (29) should be general and can be applicable to any generic distribution of impurities. Compared to sophisticated numerical methods such as NRG, the framework here is much less effort consuming and describes the Kondo effect of multi-impurity models more effectively.

C. Surface-state LDOS

As has been shown in Ref. [37], the oscillation of the Kondo temperature is strongly related to the oscillation of the surface-state LDOS. In order to cross-check this, we also calculate the LDOS from the theoretical aspect as below. In Sec. II A, we have studied the GF of the local electrons of the impurity. Now let us shift our focus to the surface conduction electrons, which gives rise to the LDOS in the standard way, as

$$\rho_s(\mathbf{x},\omega) = -\frac{1}{\pi}\mathrm{Im}G^r(\mathbf{x},\mathbf{x},\omega), \tag{30}$$

where $G^r(\mathbf{x},\mathbf{x},\omega)$ is the retarded GF of the surface electrons. For impurities adsorbed on the surface, the multiple scattering method has been proved successful [41–43]. According to the multiple scattering method, the GF is determined by the Dyson equation:

$$G^r(\mathbf{x},\mathbf{x},\omega) = G_0^r(\mathbf{x},\mathbf{x},\omega) + \sum_{i=0}^{N} G_0^r(\mathbf{x},\mathbf{x}_i,\omega)(W - i\Delta)G_i^r(\mathbf{x}_i,\mathbf{x},\omega). \tag{31}$$

$G_i^r(\mathbf{x}_i,\mathbf{x},\omega)$ can be self-consistent, calculated as follows:

$$G_i^r(\mathbf{x}_i,\mathbf{x},\omega) = G_0^r(\mathbf{x}_i,\mathbf{x},\omega) + \sum_{j\neq i}^{N} G_0^r(\mathbf{x}_i,\mathbf{x}_j,\omega)(W - i\Delta)G_j^r(\mathbf{x}_j,\mathbf{x},\omega). \tag{32}$$

$G_0^r(\mathbf{x},\mathbf{x}',\omega) = -i\pi\rho_{s0}H_0^{(1)}(k|\mathbf{x}-\mathbf{x}'|)$ is the retarded GF of free surface electrons [26,41], with $\rho_{s0} = \frac{m^*\lambda^2}{\pi\hbar^2}$ and $k = [2m^*|\omega-\omega_B|]^{1/2}/\hbar$. And $H_0^{(1)}(x)$ is the zeroth-order Hankel function of the first kind. In them, λ^2 is the area of the unit cell, ω_B is the bottom of the surface band, and m^* is the effective electron mass of the surface state. In addition, W and Δ reflect the attractive potential and hybridization, respectively [41].

For the surface state on Ag(111), the experiments reported that $\omega_B = -67$ meV and $m^* = 0.42m_e$ [50]. With the lattice constant of Ag, it can be readily derived that $\rho_{s0} = 0.125$ (1/eV). In the detailed calculation of the surface-state LDOS for Co adatom on Ag(111), $W = -0.402$ eV and $\Delta = 0.0194$ eV are incorporated. With these values, the LDOS at ε_F is calculated according to the detailed positions of the assembled adatoms. In order to compare with the experimental data, we also follow Ref. [37] to calculate the Kondo temperature according to

$$k_B T_K = \tilde{D}e^{-\frac{1}{J_b\rho_b + J_s\rho_s}}, \tag{33}$$

with effective band cutoff $\tilde{D} = 4.48$ eV, adatom–bulk-state exchange coupling $J_b = 0.51$ eV, adatom–surface-state exchange coupling $J_s = 0.225$ eV, which are experimental values obtained in Ref. [37], and with bulk-state LDOS $\rho_b = 0.27$ (1/eV) as a constant.

III. KONDO EFFECT IN THE VICINITY OF ANOTHER ADATOM ($N = 1$ CASE)

Having introduced our method, let us apply the above formalism to the simplest case, i.e., $N = 1$. Then, the sum term in the denominator of Eq. (26) as discussed above in Sec. II B will disappear. It can be simplified as

$$w \approx w_0 + \frac{A^2}{w_0}\left[Y_0^2(k_F d + \delta_s) - J_0^2(k_F d + \delta_s)\right]. \tag{34}$$

Here $Y_0(x)$ and $J_0(x)$ are the zeroth-order Bessel functions of the second and first kind, respectively. A reflects the oscillation amplitude, and δ_s is the scattering phase shift. d is the distance between the two adatoms, i.e., $R_{i0} = d$. It is worthwhile mentioning that the hybridization V_s is proportional to the overlap integral of the surface-state wave function with the localized impurity state. The surface-state wave function can be perturbed by adatoms on the surface, thus leading to some variation of the hybridization V_s. In order to reproduce realistic experimental environment, we take into account the variation of the hybridization as $V_s = e^{i\delta}V_{s0}$. V_{s0} is the unperturbed hybridization, i.e., the overlap integral of the unperturbed surface-state wave function with the localized impurity state. In general δ is a complex number with $\delta = \delta_s + i\delta_a$. Here, δ_s and δ_a are reals. Then, we can obtain $I_1(d,\omega) = AJ_0(kd + \delta_s)$ and $I_2(d,\omega) = AY_0(kd + \delta_s)$, with $A = V_{s0}^2/e^{\delta_a}$. Figure 2 shows the calculated variation of Kondo resonance width (solid red line) of two Co adatoms on Ag(111) versus the distance d between them. As a comparison, we also plot the experimental Kondo resonance width of the left adatom (black triangles) and right adatom (blue open circles) reported in Ref. [37]. In the calculation, we used the Kondo resonance width obtained for a Co adatom placed on a flat Ag(111) terrace, $w_0 = 9.8$ meV, and the surface-state Fermi wave vector of Ag(111), $k_F = 0.83$ (1/nm). In addition, we also used A and δ_s as two parameters to fit the experimental data. With $A = 9$ meV and $\delta_s = 2.2$ rad, the calculated result reproduces the experimental data reasonably well.

IV. CALCULATIONS OF THE LDOS AND THE KONDO EFFECT IN NANOCORRALS

After discussing the two-adatom case, we now move to the Kondo effect in a specific geometric configuration of

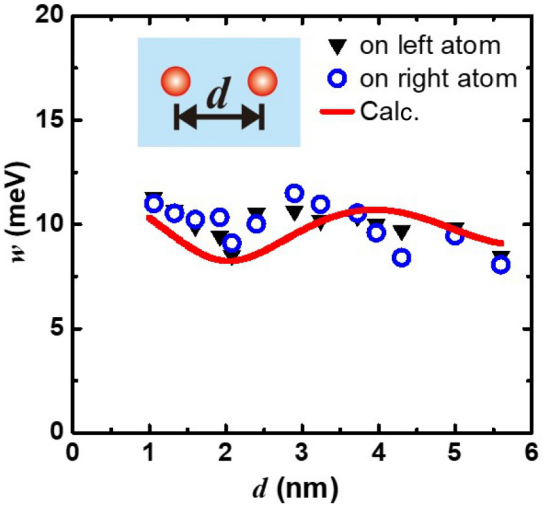

FIG. 2. Comparison between the calculated (red line) and the experimentally obtained Kondo resonance widths (black and blue symbols are from Ref. [36]) for the two-adatom case. d is the distance between the two adatoms.

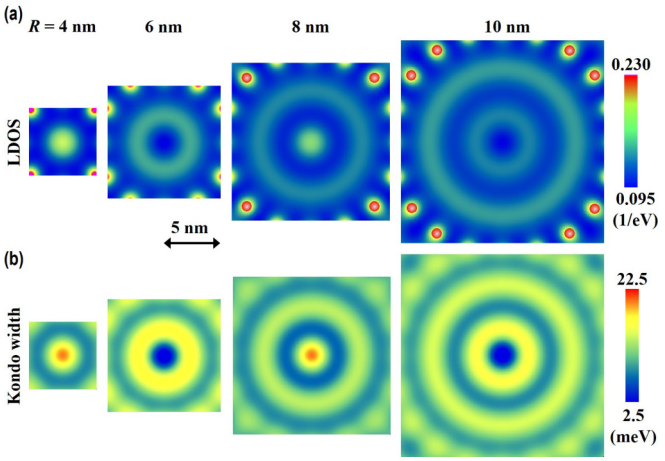

FIG. 3. The LDOS and Kondo resonance width mapping of different-sized corrals. (a) The LDOS at Fermi level for nanocorrals with different diameters. (b) The Kondo resonance width of a test Co adatom placed at an arbitrary position inside the nanocorrals with different diameters. From left to right, the corral radii are 4, 6, 8, and 10 nm, respectively. The red balls in (a) denote the positions of the Co adatoms used for building the nanocorrals.

nanocorral, where the N ($i \neq 0$) adatoms are equidistantly aligned into a quantum corral with radius R [i.e., $R_{i0} = R$ in Eq. (26)]. We first consider the LDOS of the empty corrals, i.e., no adatom inside the corrals. Figure 3(a) shows the calculated LDOS mapping inside the nanocorrals with four representative radii, 4, 6, 8, and 10 nm, respectively. The corresponding numbers of the adatoms that are used for constructing the corrals, N, are 8, 12, 16, and 20, respectively. When we compare the LDOS at the center of different corrals, we find that it shows an oscillation of bright and dark contrasts with the maximum of ∼0.20 (1/eV) and the minimum of ∼0.095 (1/eV). Moreover, the LDOS exhibits different patterns for different radii. For $R = 4$ nm, it shows a maximum at the center, while for $R = 6$ nm, the maximum evolves into a ring structure. The LDOS pattern further changes as a ring plus a maximum at the center and two ring structures for $R = 8$ and $R = 10$ nm, respectively. The finding of the LDOS variation suggests that the Kondo effect might be also position and corral radius dependent.

In order to calculate the Kondo effect, we placed another Co adatom as the test atom inside the empty corrals, namely, the corrals in Fig. 3(a). By varying the position of this test adatom inside the nanocorrals, we calculated its Kondo resonance width at arbitrary position of the corrals with different radii. Four representative results are displayed in Fig. 3(b). We note that the parameters in the two-adatom case are used here for the calculations of the Kondo effect in quantum corrals. At the center of these corrals, the Kondo resonance width has a maximum at $R = 4$ nm and a minimum at $R = 6$ nm. When R is increased to 8 nm, it becomes a maximum again. With further increasing R to 10 nm, it becomes a minimum one more time. The maximum reaches to ∼20 meV and the minimum goes down to as low as ∼2.5 meV. Inside a corral, we find that the Kondo resonance width is rotational invariant as expected from the symmetry. The maximum shows a circle for $R = 4$ nm, while it evolves into a ring structure for $R = 6$ nm. A circle plus a ring are present for $R = 8$ nm, while two rings show up for $R = 10$ nm. When comparing the calculated Kondo resonance width mapping with the LDOS mapping of the same radius shown in Fig. 3(a), we find that they show similar oscillations. This explicitly provides convincing evidence that the Kondo temperature is in general positively related to the LDOS at the Fermi level. We also note that there are also some slight differences between these two: (i) the areas in blue color (low intensity) in Fig. 3(b) are smaller than those in Fig. 3(a); (ii) a sharper transition between the blue and yellow contrast is found in Fig. 3(b) than in Fig. 3(a). These suggest a nonlinear relation between them, which is different from the linear relation claimed in Ref. [30]. Further detailed information and the comparison between the calculated results with the experimental data will be given in the next section.

V. COMPARISON WITH EXPERIMENTS

A. LDOS and Kondo effect for adatoms at corral centers

In this section, we show a one-to-one comparison between our calculations and the experimental results. We first extract the LDOS at the center of different empty corrals [Fig. 3(a)], and plot it as a function of the corral radius. The blue curve in Fig. 4(a) shows the calculated results with the scale shown at the right side. With enlarging the corral radius from ∼3 to ∼10.5 nm, the LDOS displays a decayed oscillation with a period of ∼3.8 nm, which is the half Fermi wavelength of the surface-state electrons. We also plot the calculated Kondo resonance width for a Co adatom placed at the corral centers as a function of the corral radius in Fig. 4(b) (red curve). It shows that the Kondo resonance width also exhibits an oscillation as the function of the corral radius. The first peak appears at ∼4 nm, and the second peak appears at ∼7.8 nm. The oscillation period exactly matches with the half Fermi wavelength of the surface-state electrons. To make comparisons with experiments, we also plot both the experimentally obtained dI/dV and w (black symbols) from Ref. [37] in their corresponding figures. We find that the calculated results reproduce the oscillating behaviors of the experiments. In addition, the calculated Kondo resonance decays slower than that observed in experiments. This may be attributed to the surface-state lifetime effect [51–53], which is not considered in the above calculations.

Apart from the Kondo resonance width calculation with Eq. (26), we also used the calculated LDOS to further estimate the Kondo resonance width using Eq. (33), the blue curve in Fig. 4(b). It also exhibits a decayed oscillating behavior that agrees well with the experiments. We note that there is a minor difference in terms of a lateral shift between the calculated results and experimental ones. This may be due to the LDOS perturbation caused by the test Co adatoms in the corral center. The adding of the test adatom can cause a phase shift in the LDOS while this effect was not considered in the LDOS calculation since it was derived only for the empty corrals. Essentially, the oscillations of the Kondo resonance width are clearly revealed by the variations of the surface-state LDOS.

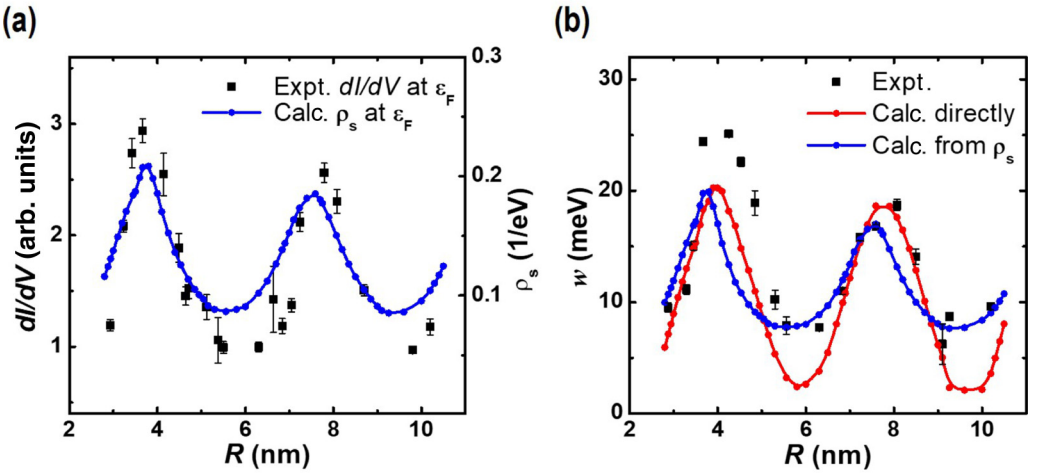

FIG. 4. The corral radius-dependent LDOS and Kondo resonance width at the center of the nanocorrals. (a) The calculated LDOS (blue curve) and experimental *dI/dV* (black squares) varied with *R*. (b) The corral radius-dependent Kondo resonance width. The red curve is the calculation according to Eq. (26). The blue curve is the calculation according to Eq. (33). The experimental data (black squares) are from Ref. [36].

B. LDOS and Kondo effect for adatom placed at arbitrary positions inside nanocorrals

As shown in Figs. 3(a) and 3(b), both the LDOS and the Kondo resonance width of the test adatom inside a corral exhibit the spatial variation. To describe this feature more quantitatively, and to further identify the validity of the calculated results, we first selected the calculated results of two representative nanocorrals. Then we performed the position-dependent LDOS and Kondo resonance width measurements for the Co adatom placed inside the corrals under the same experimental conditions mentioned in Ref. [37]. The Fano formula was again utilized to extract the Kondo resonance width. Figures 5(a) and 5(b) show the topography of the empty corral and a Co adatom placed with a separation r away from the corral center, respectively. The measured r-dependent *dI/dV* spectra at the Fermi level for $R = 9.1$ nm and 7.2 nm are plotted as black squares in Figs. 5(c) and 5(e), respectively. The curves clearly display oscillations. While a maximum is found at the center of the corral for $R = 7.2$ nm, a minimum is present at the center point for $R = 9.1$ nm. As a comparison, the calculated LDOSs of the surface state are plotted as the blue curve in Figs. 5(c) and 5(e), which show excellent agreement with the experimentally obtained *dI/dV* (solid squares). The experimentally measured Kondo resonance width for a Co adatom as a function of the distance r away from the corral center is shown as black squares in Figs. 5(d) and 5(f) for $R = 9.1$ nm and $R = 7.2$ nm, respectively. They exhibit almost the same oscillating behavior with the LDOS. The calculated results utilizing Eq. (26) for the Kondo resonance width inside the corral are shown as red curves in Figs. 5(d) and 5(f), respectively. They show oscillating behaviors, and match with the experimental results. The Kondo temperature obtained from the calculated surface-state LDOS by Eq. (33) is also shown as blue curves in Figs. 5(d) and 5(f), respectively. We can see that they can also reproduce the oscillation behavior of experimental data. The two methods here both provide their own abilities to describe the Kondo effect. The above

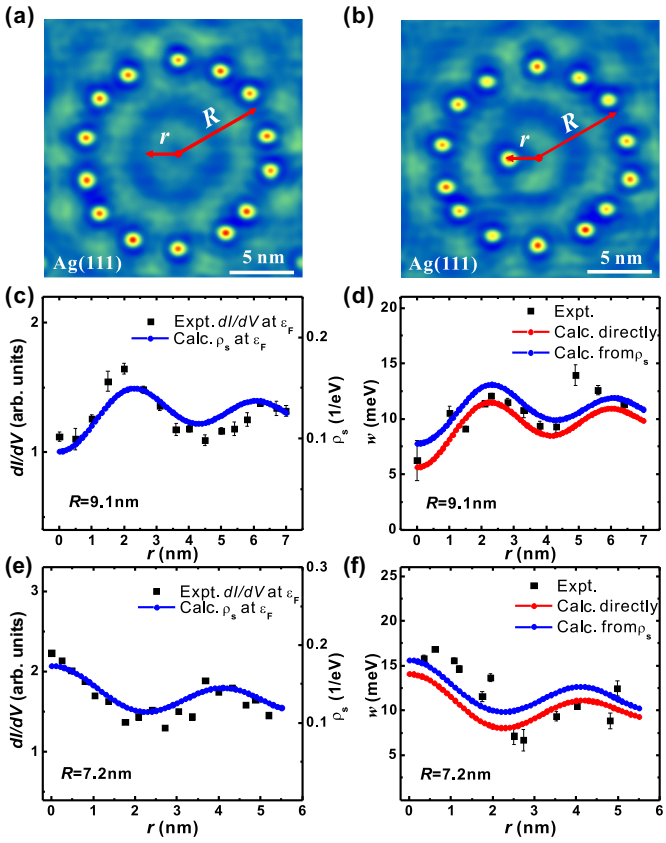

FIG. 5. The LDOS and Kondo resonance width of a Co adatom located at a position with the distance r away from the corral center. (a,b) are topographic images of a quantum corral without and with a Co atom in the corral, respectively. (c) is the comparison between the experimentally obtained *dI/dV* (black squares) and the calculated LDOS (blue line), and (d) is the comparison between the experimentally obtained Kondo resonance width (black squares) and theoretically calculated ones (red and blue lines) for a corral with $R = 9.1$ nm. (e,f) are similar comparisons as (c,d) but for a corral with $R = 7.2$ nm.

one-to-one comparisons show that the calculations reproduce the experimental data well for different-radius corrals. These demonstrate that our method provides an effective way for dealing with the Kondo effect in multiple-impurity systems.

It is worth mentioning that the Kondo resonance widths of the adatoms located at the corral edge show no apparent difference with that of a single isolated Co adatom on Ag(111). Both the experiments and calculations confirm this finding. This can be understood since the standing wave needs to form a knot at the corral edge, resulting in only minor variation of the surface-state LDOS at Fermi energy and subsequently the Kondo resonance width.

VI. SUMMARY

We developed a Green's function based method to calculate the Kondo resonance width of a magnetic adatom placed on a substrate with surface state and surrounded by multiple adatoms. We applied the method to calculate the Kondo resonance width of a test Co atom placed at arbitrary positions inside nanocorrals formed by Co adatoms on a Ag(111) surface. Our calculations not only reproduced the recently reported Kondo resonance width oscillation as a function of the corral diameter but also predicted that the Kondo resonance width also oscillates as the function of its separation from the corral center. The prediction is further confirmed by the low-temperature scanning tunneling microscopy studies where a one-to-one correspondence is found. The good agreement with the experiments validates the generality of the method to the system where multiadatoms are involved. Our calculations also reveal a strong correlation between the Kondo resonance width and the surface LDOS at ε_F. Though the calculations were made for the Co/Ag(111) system here, it can be straightforwardly applied to other experimental setups, such as the Kondo effect in the resonator and rectangle geometry structures, which have been experimentally studied [41,54].

ACKNOWLEDGMENTS

This work was supported by the National Key R&D Program of China (Grant No. 2017YFA0303202), the National Natural Science Foundation of China (Grants No. 51571109, No. 11734006, No. 51601087, and No. 11374145), and the Natural Science Foundation of Jiangsu Province (Grant No. BK20150565).

Q.L.L. and R.W. contributed equally to this work.

[1] A. C. Hewson, *The Kondo Problem to Heavy Fermions* (Cambridge University Press, Cambridge, UK, 1993).
[2] W. J. de Haas, J. de Boer, and G. J. van dën Berg, Physica (Amsterdam) **1**, 1115 (1934).
[3] J. Kondo, Prog. Theor. Phys. **32**, 37 (1964).
[4] A. A. Abrikosov, Physics **2**, 5 (1965).
[5] H. Suhl, Phys. Rev. **138**, A515 (1965).
[6] V. Madhavan, W. Chen, T. Jamneala, M. F. Crommie, and N. S. Wingreen, Science **280**, 567 (1998).
[7] H. C. Manoharan, C. P. Lutz, and D. M. Eigler, Nature **403**, 512 (2000).
[8] N. Knorr, M. A. Schneider, L. Diekhöner, P. Wahl, and K. Kern, Phys. Rev. Lett. **88**, 096804 (2002).
[9] K. Nagaoka, T. Jamneala, M. Grobis, and M. F. Crommie, Phys. Rev. Lett. **88**, 077205 (2002).
[10] J. Li, W.-D. Schneider, R. Berndt, and B. Delley, Phys. Rev. Lett. **80**, 2893 (1998).
[11] A. Zhao, Q. Li, L. Chen, H. Xiang, W. Wang, S. Pan, B. Wang, X. Xiao, J. Yang, J. G. Hou, and Q. Zhu, Science **309**, 1542 (2005).
[12] Y.-S. Fu, S.-H. Ji, X. Chen, X.-C. Ma, R. Wu, C.-C. Wang, W.-H. Duan, X.-H. Qiu, B. Sun, P. Zhang, J.-F. Jia, and Q.-K. Xue, Phys. Rev. Lett. **99**, 256601 (2007).
[13] V. Iancu, A. Deshpande, and S.-W. Hla, Phys. Rev. Lett. **97**, 266603 (2006).
[14] J. Kügel, M. Karolak, A. Krönlein, J. Senkpiel, P.-J. Hsu, G. Sangiovanni, and M. Bode, Phys. Rev. B **91**, 235130 (2015).
[15] S. Meierott, N. Néel, and J. Kröger, Phys. Rev. B **91**, 201111 (2015).
[16] J. Kugel, M. Leisegang, M. Bohme, A. Kronlein, A. Sixta, and M. Bode, Nano Lett. **17**, 5106 (2017).
[17] V. S. Stepanyuk, N. N. Negulyaev, L. Niebergall, R. C. Longo, and P. Bruno, Phys. Rev. Lett. **97**, 186403 (2006).
[18] R. X. Cao, B. F. Miao, Z. F. Zhong, L. Sun, B. You, W. Zhang, D. Wu, A. Hu, S. D. Bader, and H. F. Ding, Phys. Rev. B **87**, 085415 (2013).
[19] J. Hu, R. X. Cao, B. F. Miao, Z. Liu, Z. F. Zhong, L. Sun, B. You, D. Wu, W. Zhang, A. Hu, S. D. Bader, and H. F. Ding, Surf. Sci. **618**, 148 (2013).
[20] R. X. Cao, Z. Liu, B. F. Miao, L. Sun, D. Wu, B. You, S. C. Li, W. Zhang, A. Hu, S. D. Bader, and H. F. Ding, Phys. Rev. B **90**, 045433 (2014).
[21] R. X. Cao, L. Sun, B. F. Miao, Q. L. Li, C. Zheng, D. Wu, B. You, W. Zhang, P. Han, S. D. Bader, W. Y. Zhang, and H. F. Ding, Sci. Rep. **5**, 12092 (2015).
[22] V. S. Stepanyuk, L. Niebergall, W. Hergert, and P. Bruno, Phys. Rev. Lett. **94**, 187201 (2005).
[23] A. T. Ngo, E. H. Kim, and S. E. Ulloa, Phys. Rev. B **95**, 161407 (2017).
[24] C. R. Moon, C. P. Lutz, and H. C. Manoharan, Nat. Phys. **4**, 454 (2008).
[25] J. Kliewer, R. Berndt, and S. Crampin, Phys. Rev. Lett. **85**, 4936 (2000).
[26] O. Agam and A. Schiller, Phys. Rev. Lett. **86**, 484 (2001).
[27] A. A. Aligia, Phys. Rev. B **64**, 121102 (2001).
[28] G. A. Fiete, J. S. Hersch, E. J. Heller, H. C. Manoharan, C. P. Lutz, and D. M. Eigler, Phys. Rev. Lett. **86**, 2392 (2001).
[29] D. Porras, J. Fernández-Rossier, and C. Tejedor, Phys. Rev. B **63**, 155406 (2001).
[30] E. Rossi and D. K. Morr, Phys. Rev. Lett. **97**, 236602 (2006).
[31] L. Limot and R. Berndt, Appl. Surf. Sci. **237**, 576 (2004).
[32] J. Merino and O. Gunnarsson, Phys. Rev. Lett. **93**, 156601 (2004).
[33] C. Y. Lin, A. H. Castro Neto, and B. A. Jones, Phys. Rev. B **71**, 035417 (2005).

[34] M. A. Schneider, P. Wahl, L. Diekhöner, L. Vitali, G. Wittich, and K. Kern, Jpn. J. Appl. Phys. **44**, 5328 (2005).
[35] C. Y. Lin, A. H. Castro Neto, and B. A. Jones, Phys. Rev. Lett. **97**, 156102 (2006).
[36] J. Henzl and K. Morgenstern, Phys. Rev. Lett. **98**, 266601 (2007).
[37] Q. L. Li, C. Zheng, R. Wang, B. F. Miao, R. X. Cao, L. Sun, D. Wu, Y. Z. Wu, S. C. Li, B. G. Wang, and H. F. Ding, Phys. Rev. B **97**, 035417 (2018).
[38] P. W. Anderson, Phys. Rev. **124**, 41 (1961).
[39] C. Kolf and J. Kroha, Phys. Rev. B **75**, 045129 (2007).
[40] K. G. Wilson, Rev. Mod. Phys. **47**, 773 (1975).
[41] J. Fernández, M. Moro-Lagares, D. Serrate, and A. A. Aligia, Phys. Rev. B **94**, 075408 (2016).
[42] G. A. Fiete and E. J. Heller, Rev. Mod. Phys. **75**, 933 (2003).
[43] K. Wildberger, V. S. Stepanyuk, P. Lang, R. Zeller, and P. H. Dederichs, Phys. Rev. Lett. **75**, 509 (1995).
[44] J. R. Schrieffer and P. A. Wolff, Phys. Rev. **149**, 491 (1966).
[45] P. Wahl, P. Simon, L. Diekhoner, V. S. Stepanyuk, P. Bruno, M. A. Schneider, and K. Kern, Phys. Rev. Lett. **98**, 056601 (2007).
[46] A. Spinelli, M. Gerrits, R. Toskovic, B. Bryant, M. Ternes, and A. F. Otte, Nat. Commun. **6**, 10046 (2015).
[47] A. Schiller and S. Hershfield, Phys. Rev. B **61**, 9036 (2000).
[48] M. Plihal and J. W. Gadzuk, Phys. Rev. B **63**, 085404 (2001).
[49] U. Fano, Phys. Rev. **124**, 1866 (1961).
[50] J. Li, W.-D. Schneider, and R. Berndt, Phys. Rev. B **56**, 7656 (1997).
[51] J. Li, W.-D. Schneider, R. Berndt, O. R. Bryant, and S. Crampin, Phys. Rev. Lett. **81**, 4464 (1998).
[52] J. Kliewer, R. Berndt, E. V. Chulkov, V. M. Silkin, P. M. Echenique, and S. Crampin, Science **288**, 1399 (2000).
[53] S. Heers, P. Mavropoulos, S. Lounis, R. Zeller, and S. Blügel, Phys. Rev. B **86**, 125444 (2012).
[54] S. Crampin, H. Jensen, J. Kröger, L. Limot, and R. Berndt, Phys. Rev. B **72**, 035443 (2005).